

# Trapping of $C_2^-$ in a digital ion trap

Alexander Hinterberger, Sebastian Gerber , Emanuel Oswald, Christan Zimmer, Julian Fesel and Michael Doser

CERN, European Laboratory for Particle Physics, 1211 Geneva, Switzerland

E-mail: [sebastian.gerber@cern.ch](mailto:sebastian.gerber@cern.ch)

Received 10 July 2019, revised 2 September 2019

Accepted for publication 30 September 2019

Published 25 October 2019



CrossMark

## Abstract

In this article we present the production of a pulsed molecular  $C_2^-$  beam and the subsequent trapping of  $C_2^-$  in a digital ion trap (DIT). The anionic molecules were produced in a pulsed discharge valve from acetylene and carbon dioxide gas in a helium carrier. The mass spectrum of the pulsed anion beam is initially recorded using a Wien filter. Subsequently, we measured the mass spectrum using the DIT and its stability diagram. The results are compared to a theoretical description of the trap's stability conditions. The research is relevant for future laser cooling experiments of trapped  $C_2^-$  and for sympathetic cooling experiments of other anionic species (antiprotons, electrons, anionic atoms and molecules) and are of interest for precision experiments on antihydrogen as performed at the antiproton decelerator facility at CERN.

Keywords: digital ion trap, molecular anion, supersonic gas expansion, mass spectrum,  $C_2^-$

(Some figures may appear in colour only in the online journal)


## 1. Introduction

Molecular and atomic anions are of importance in a range of fields, including astrophysics [1] and research on the interstellar medium [2], chemistry of correlated systems [3–5] and negative superhalogens [6]. In order to study the processes at energies at which anions play a role, it is necessary to synthesize them under well defined conditions and cool them to ultracold temperatures. Currently, temperatures of at best several Kelvin have been achieved in supersonic gas expansions followed by buffer gas cooling (or electron cooling in the case of antiprotons in Penning traps) in cryogenic environments [7–9].

Laser cooling techniques, which are routinely used for neutral atoms and positive ions (in Paul or Penning traps) as well as for neutral molecules like YO, CaF and SrF [10–12], have the potential to reach sub-Kelvin temperatures. However, so far this has never been achieved for anions [13]. Laser cooling of one anionic species would in principle allow to sympathetically cool any other negatively charged system, including atomic and molecular anions, electrons and

antiprotons. The latter has recently sparked attention for antihydrogen experiments as the sensitivity of precision spectroscopic [14, 15] and planned precision gravitational measurements [16] depend on the temperature at which the antiatoms are investigated. Measuring the gravitational interaction between matter and antimatter with similar precision as has been accomplished for matter experiments [17], requires the full control of internal and external states of antiatoms and energies below  $\mu\text{eV}$ . Laser cooling of anions (and sympathetic cooling of antiprotons) in Paul and Penning traps has the potential to reach these working conditions. The temperature at which antihydrogen can be formed via resonant charge exchange of antiprotons with ortho-positronium is potentially only constrained by the recoil limit of the constituents [16]. The goal of creating ultracold antihydrogen via this approach has sparked theoretical and experimental investigations surrounding the use of laser-cooled atomic anions like  $\text{Os}^-$  and  $\text{La}^-$  [18, 19]. Very recently, trapping of such atomic anions in a Paul trap has been shown [20].

Given the challenges inherent in laser cooling atomic anions, the prospect of using molecular candidates was investigated in parallel [21–23]. Here it was found that  $C_2^-$  is a good candidate with the advantage of a known level structure and a well suited branching ratio between the A and X ground vibrational state of 96%. Further,  $C_2^-$  exhibits neither hyperfine structure nor unwanted photodetachment when

 Original content from this work may be used under the terms of the [Creative Commons Attribution 3.0 licence](https://creativecommons.org/licenses/by/3.0/). Any further distribution of this work must maintain attribution to the author(s) and the title of the work, journal citation and DOI.

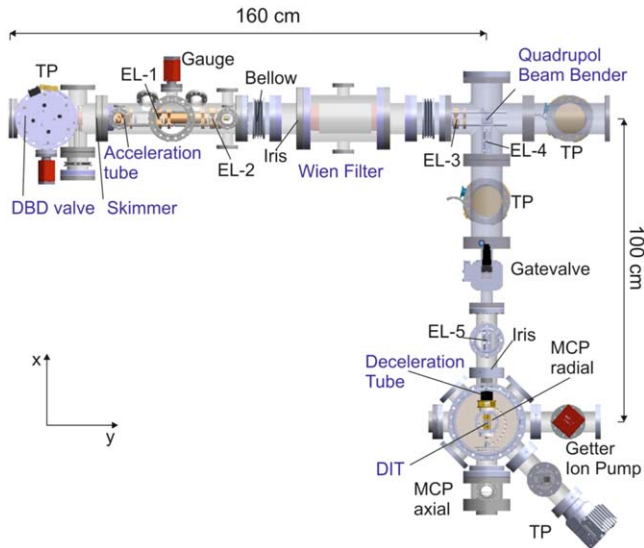


**Figure 1.** Sketch and CAD drawing of the experimental setup with its dimensions given in the horizontal  $x$ - $y$  plane. Anions produced by the Even-Lavie DBD valve pass the skimmer, acceleration tube, electrostatic optics of Einzel lenses (EL 1-5), Wien filter with two irises and a quadrupole beam bender before they are decelerated, trapped in the DIT, radially extracted and detected on the MCP. The vacuum is maintained with one getter ion and four turbo pumps (TP).

addressing the A to X transition [21]. In this article we describe an experimental setup to produce  $C_2^-$ , with potentially cold internal energies, from supersonic gas expansion, to form a pulsed beam of  $C_2^-$ . The  $C_2^-$  beam is then decelerated and trapped in a digital ion trap (DIT) as a first step towards laser cooling of trapped  $C_2^-$ .

## 2. Experimental setup

The experimental setup is sketched in figure 1. Anions are produced from a gas mixture of 5%  $C_2H_2$ , 3%  $CO_2$  in a He carrier at 10 bar using a supersonic expansion valve of the Even-Lavie type with an installed dielectric barrier discharge stage. Details of the valve can be found in [9, 24, 25]. The discharge is seeded by electrons released at 20 eV from a biased glow cathode mounted 10 cm below the valve.

After expansion, part of the gas cloud passes a 3 mm skimmer (Ni, BeamDynamics) located 17 cm downstream of the valve. Behind the skimmer, only the anions in the gas cloud are accelerated in a pulsed tube of 4 cm length and 3 cm diameter mounted between two 93% transmission Au meshes.

By varying the timing of the pulsing, the particle velocity behind the valve (before acceleration) is determined to be  $\sim 750 \text{ m s}^{-1}$ ; the pulse duration is 30  $\mu\text{s}$ . The pulsed tube is ramped in the range of  $V_{\text{acc}} = -1$  to  $-2$  kV using a push-pull switch and the anions are accelerated while exiting the tube towards a grounded Au mesh mounted 1.5 cm downstream. The accelerated anions then pass two four fold-segmented Einzel lenses before they are mass-selected in a Wien filter (Beam Imaging Solutions, 600-H) with a nominal resolution

of  $m/\Delta m \sim 400$ . For this the Wien filter is mounted on the beam axis between a front 4 mm and a back 6 mm iris. The Wien filter mass selection is described in more detail in [26]. Behind the filter, the anion beam is sent through a  $90^\circ$  quadrupole beam bender and guided towards a resistive tube (Photonis Inc.) by means of three Einzel lenses. Here, the anions are decelerated to energies required for trapping. The resistive tube's entrance is located  $\sim 1.3$  m after the Wien filter and a 7 mm iris at its entrance can select a desired mass range depending on the filter's current and voltage settings. The resistive tube itself consists of a 9 cm glass cylinder which is coated on the inside with a resistive ink resulting in  $30 \text{ M}\Omega$  between its ends. The tube is clamped between two parallel polished metal plates with Au meshes perpendicular to the beam axis. Applying a potential difference of ground to  $V_{\text{float}}$  between the two plates creates a homogeneous electric field that decelerates the anions. Finally, about 5% of the total anions exit the tube with a remaining energy of up to 25 eV with  $\sim 0.5\%$  below 1 eV.

The DIT is directly behind the exit of the resistive tube, where figure 2 shows the CAD drawings in two planes. The pressure inside the trap chamber reaches  $3 \times 10^{-9}$  mbar. The trap itself consists of four stainless steel rods each with 8 mm diameter and a distance of  $r_0 = 3.5$  mm between the rod surface and the center of the trap. The design consists of two sections, where the first acts as an rf guide for the decelerated anions and has a length of 40 mm. The second part constitutes the trap and incorporates two end-cap electrodes for the axial enclosure with a distance from the center of  $z_0 = 10$  mm. The end-caps, as shown in figure 2, are mounted around the rods and have electrodes that reach between the rods in order to leave out a hole of 5 mm radius in the middle. They are controlled by a push-pull switch between  $V_{\text{float}}$  and  $V_{\text{ax}}$  to allow capture of the anion bunch. During the experiment the typical end cap voltage is  $V_{\text{ax}} = V_{\text{float}} - 100$  V. The four rf rods are digitally driven in two operation modes using a four-channel push-pull switch (CGC, AMX250-4E) supplied by a positive  $V_{\text{pos}}$  and negative  $V_{\text{neg}}$  supply voltage (Delta Elektronika, SM 300 10D) which are floated to  $V_{\text{float}}$ . Four 93  $\Omega$  BNC cables each 40 cm were used to connect the switch to the vacuum feedthrough. The overall capacitance from the cables, feedthrough and the trap electrodes and in-vacuum lines is approximately 50 pF. This results in rise times of the trap voltages of about 300 ns and limits the rf drive to operate at a peak-to-peak voltage of 250 V at 3 MHz. The rms voltage noise on the trap electrodes is approximately given by the power supplies to about 10 mV.

In kick-out mode,  $V_{\text{neg}}$  is applied to the two lower rods and  $V_{\text{pos}}$  to the upper rods. By that the anions are extracted radially from the trap towards a two-stage micro-channel plate (MCP, HAMAMATSU F1112-P47) detector coupled to a phosphor screen and read by a CMOS camera. The MCP is mounted 4 cm above the trap and behind a grounded Au mesh. In trapping mode, a periodic rectangular waveform with peak-to-peak voltage  $V_{\text{rf}} = (V_{\text{pos}} - V_{\text{neg}})$  is applied to two diagonal rods, with the neighboring rods phase shifted by  $\pi$ . The change from trapping to kick-out mode takes one trap-cycle, which is  $\sim 300$  ns at 3 MHz. The stability parameters

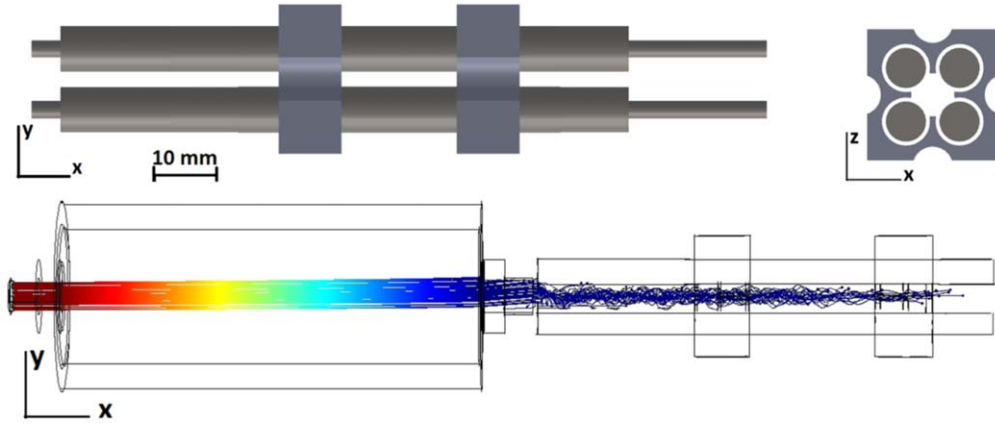


**Figure 2.** (Upper) Side and front view of a CAD drawing showing the DIT, the four rf guides and trap-rods (gray) and the endcap electrodes (blue). (Lower) COMSOL simulation of the decleration tube and the DIT in guiding mode with  $V_{\text{acc}} = 1800$  V,  $V_{\text{float}} = 1795$  V,  $V_{\text{ax}} = 0$  V, and  $d = 0.5$  and initial particles' radial energy of 1 eV. The color code from red to blue corresponds to the kinetic energy.

when operating in trapping mode can be expressed as solutions to the Mathieu equation as [27]

$$\begin{aligned} a_y &= -a_x = -\frac{8eU_{\text{dc}}}{m\Omega^2 r_0^2}, \\ -q_y &= q_x = -\frac{2eV_{\text{rf}}}{m\Omega^2 r_0^2}, \end{aligned} \quad (1)$$

where  $\Omega = 2\pi/T$  is the frequency and  $T$  is the period of the rectangular wave, which is divided into two sub-periods  $T = \tau_1 + \tau_2$ . To simulate the dc- $U_{\text{dc}}$  and the ac-component  $V_{\text{rf}}$  for a mass spectrum in a DIT, the duty cycle  $d$  can be defined as  $d = \frac{\tau_1}{T}$  with  $\tau_1$  the part of the period where the waveform has  $V_{\text{pos}}$  (and  $\tau_2 = T - \tau_1$  the part of the period that has  $V_{\text{neg}}$ ). The voltage components are then expressed as a function of the duty cycle and the supplied voltages by [28]

$$\begin{aligned} U_{\text{dc}} &= dV_{\text{pos}} + (1 - d)V_{\text{neg}}, \\ V_{\text{rf}} &= 2(V_{\text{pos}} - V_{\text{neg}})(1 - d)d. \end{aligned} \quad (2)$$

The trap depth of a DIT can be calculated as [29]

$$\begin{aligned} \phi_{\text{sec}}(r_0) &= c \frac{e^2}{2m\Omega^2} \frac{V_{\text{rf}}^2}{r_0^2} - \frac{\mu e V_{\text{ax}} r_0^2}{2z_0^2}, \\ c &= \frac{1}{2} \sum_{n=1}^{\infty} \frac{a_n^2}{n^2}, \\ a_n &= \frac{4}{\pi n} \sin(n\pi\tau). \end{aligned} \quad (3)$$

Here,  $\mu$  is a geometrical factor with a value of approximately 0.25 [29]. For the case of an anion with mass  $m = 24$  u and charge  $-e$ , and using  $d = 0.5$  which gives  $\tau = T/2$ , the digital trap's depth becomes  $\phi_{\text{sec}} \approx 22.37$  eV (3).

A typical deceleration and guiding event of an anion bunch of 30  $\mu\text{s}$  in length is visualized using COMSOL in figure 2. Entering particles are decelerated by the homogeneous electric field inside the tube. Once the particles pass the last Au-mesh their trajectory is influenced by the rf guide. The deceleration and trapping efficiency depends on the initial radial kinetic energy of the particles, their space charge and the experimental alignment of the parts.

For a stable trap operation, the Mathieu parameters can be calculated using a matrix approach for the numerical solution of the Hill equation [30]. A detailed description of this method can be found in [30–34].

Since the applied rf voltage in a DIT is approximately constant during a time segment  $\tau_n$  with  $n = 1, 2$ , the anion's velocity and position can be defined for the entire cycle  $T$ . In the positive and negative voltage case, the transfer matrices  $V_1$  and  $V_2$  can be written as

$$V_n = \begin{cases} \begin{pmatrix} \cos(\tau_n \sqrt{f_n}) & \frac{\sin(\tau_n \sqrt{f_n})}{\sqrt{f_n}} \\ -\sin(\tau_n \sqrt{f_n}) \sqrt{f_n} & \cos(\tau_n \sqrt{f_n}) \end{pmatrix}, & f_n > 0 \\ \begin{pmatrix} \cosh(\tau_n \sqrt{-f_n}) & \frac{\sinh(\tau_n \sqrt{-f_n})}{\sqrt{-f_n}} \\ \sinh(\tau_n \sqrt{-f_n}) \sqrt{-f_n} & \cosh(\tau_n \sqrt{-f_n}) \end{pmatrix}, & f_n < 0, \end{cases} \quad (4)$$

with  $\tau_n = d\pi$ ,  $f_n = a + \epsilon_n 2q$  and  $\epsilon_n \in \{1, -1\}$ . Equation (4) is then independently calculated for the radial directions  $x$  and  $y$  using the relation  $f_n(x) = -f_n(y)$  [30]. Stable particle trajectories in  $x$  or  $y$  direction in the  $a, q$  Mathieu parameter space are possible when the trace of the product  $M = V_1 \cdot V_2$  is less than two [33, 34]:

$$|\text{Tr}(M)| < 2. \quad (5)$$

A stable trap operation is then given when the stability condition of equation (5) is fulfilled for both radial directions. The enclosure in  $z$  direction requires two end caps with negative voltage. With these equations the shape of the stability diagram can be plotted.

Variation of one experimental parameter, e.g. the trap frequency  $\Omega$  or the rf amplitude  $V_{\text{rf}}$ , while leaving the others unchanged, causes the resulting  $a, q$  values in equation (1) to line up along a certain working slope, which is given by the ratio

$$\frac{a}{q} = \frac{2U_{\text{dc}}}{V_{\text{rf}}} = \frac{2d - 1}{4d(1 - d)}, \quad (6)$$

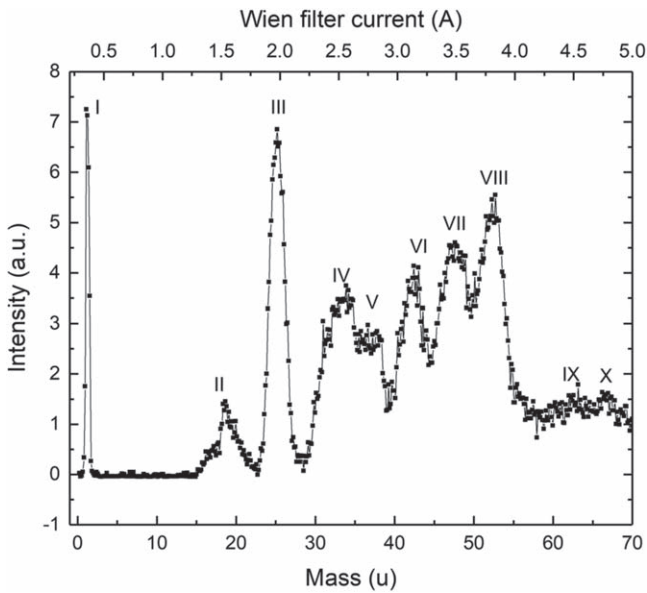


**Figure 3.** Mass to charge anion spectrum intensity at  $V_{\text{acc}} = -1740$  V versus the Wien filter current (upper axis) in 10 mA steps while the Wien filter voltage is kept constant at 160 V. The lower axis represents the mass spectrum for  $Z = 1-70$  u. The different peaks labeled in the spectrum most likely contain (I):  $\text{H}^-$ , (II):  $\text{CH}_3^-$ ,  $\text{O}^-$ ,  $\text{OH}^-$ ,  $\text{H}_2\text{O}^-$ , (III):  $\text{C}_2^-$ ,  $\text{C}_2\text{H}^-$ ,  $\text{H}_2\text{CC}^-$ , (IV):  $\text{O}_2^-$ , (V):  $\text{C}_3\text{H}_x^-$ , (VI):  $\text{C}_3\text{H}_y^-$ , (VII):  $\text{C}_4\text{H}_x^-$ , (VIII):  $\text{C}_4\text{H}_y^-$ , (VIII), (IX), (X):  $\text{C}_2\text{H}_z^-$

where the working slope can be defined by the duty cycle  $d$  using equation (2). The working slope is then typically used in experiments to obtain a mass spectrum of the trapped particles, as discussed in the next section.

### 3. Experimental results

To characterize and optimize the pulsed valve production of anions we recorded a mass spectrum behind the Wien filter stage and the quadrupole beam bender, which is shown in figure 3 from 1 u up to 70 u. The beam intensity was recorded with the MCP and each data point comprises the detected particles after one valve shot. The spectrum depicts a distinct peak at 1 u, likely coming from  $\text{H}^-$  [35], which has a contribution to the total intensity of about 3%. The peak around mass 18–20 u probably contains stable  $\text{O}^-$  [36],  $\text{OH}^-$  [37] and  $\text{H}_2\text{O}^-$  [38], corresponding to about 5% of the total intensity. Then, several peaks at different carbon hydrate compositions are visible for  $\text{CH}_x^-$ , and  $\text{C}_2\text{H}_x^-$ . The peaks larger than 30 u most likely consist of components of  $\text{C}_3\text{H}_x^-$  and  $\text{C}_4\text{H}_x^-$  and of clusters of anionic acetylene molecules, whose formation is described in [9, 39]. A signal at the masses of stable anions such as  $\text{CO}^-$  [40] or  $\text{O}_2^-$  [41] is visible as well, with probably a small contribution of the short-lived  $\text{CO}_2^-$  [42]. Here we find that about 75% of all anionic molecules are produced with masses above 30 u. The sought-after species  $\text{C}_2^-$  is contained in the second large peak, which is about 17% of the total intensity. This peak further contains the stable molecules  $\text{C}_2\text{H}^-$  [43] and  $\text{H}_2\text{CC}^-$  [44], while the molecule  $\text{C}_2\text{H}_2^-$  is unstable [45]. To increase the  $\text{C}_2^-$

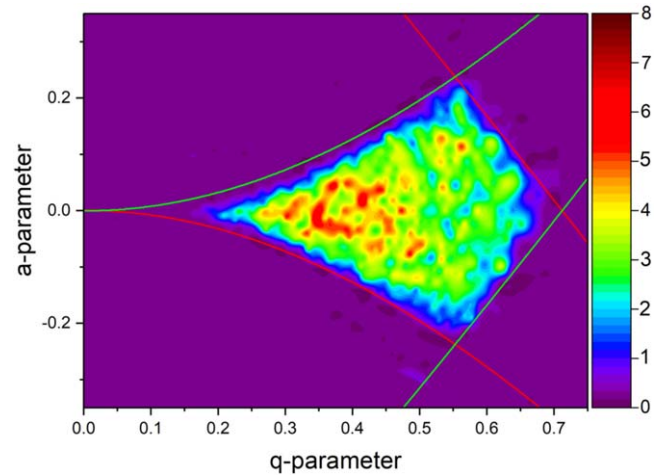


**Figure 4.** Measured stability diagram for the DIT. The color plot corresponds to the measured, relative MCP intensities, with the scale given on the right side of the plot. The region of stable solutions determined by equation (4) is marked in green lines for  $y$ -stability and red lines for  $x$ -stability.

yield, we tested several gas mixtures by varying the concentration of  $\text{C}_2\text{H}_2$  and  $\text{CO}_2$  in Ne, Ar and He. We found a maximum yield at the used mixture of 5%  $\text{C}_2\text{H}_2$  and 2%  $\text{CO}_2$  in He. Higher seed gas concentrations did not result in more particles, most likely due to preferential formation of clusters [9].

The peak around mass 25 u was selected by a Wien filter current of 1.945 A and decelerated towards the DIT. Here we first recorded the trap's stability diagram to deduce the solutions of the Mathieu equation. For this the anions were trapped for a duration of 0.2 ms, before being radially extracted and sent to a grounded Au mesh and the MCP.

To map the parameter space from  $q = 0$  to  $q = 0.44$ , the rf amplitude was increased from 0 to  $V_{\text{rf}} = 248$  V at constant  $\Omega/2\pi = 3$  MHz. To record from  $q = 0.44$  to  $q = 0.72$  the frequency was lowered from 3 to 2.36 MHz at a constant  $V_{\text{rf}} = 248$  V. To scan the  $a$ -axis,  $d$  was varied from 0.36 to 0.64. Figure 4 shows the MCP recorded intensity plotted in an  $a$ ,  $q$  diagram for mass 24 u together with the theoretical prediction for stable orbits. The edges of the measured diagram follow approximately the theoretical stability criteria, which are calculated using equation (4). Here equation (4) is calculated from  $a = -0.4$  to 0.4 and  $q = 0-0.8$  in 900 steps each, yielding a total of  $8.1 \times 10^5$  points. For each point the stability conditions have been calculated from equation (5) in  $x$  and  $y$  direction and the limits have been indicated. For the area enclosed by these lines the stability conditions are fulfilled. We further measured an increase of the relative particle numbers in the region around  $q \approx 0.35$  and  $a = \pm 0.05$ . These are expected parameters for an optimal trap operation [29].

Subsequently, we recorded an  $m/z$  spectrum by adjusting the parameters for trap operation at the upper edge of the stability diagram at  $d = 0.6$  (about  $q = 0.553$ ,  $a = 0.205$ ). The spectrum is shown in figure 5, where we scanned  $\Omega$ , while leaving the other trap parameters unchanged. Each data point corresponds to the MCP intensity after background

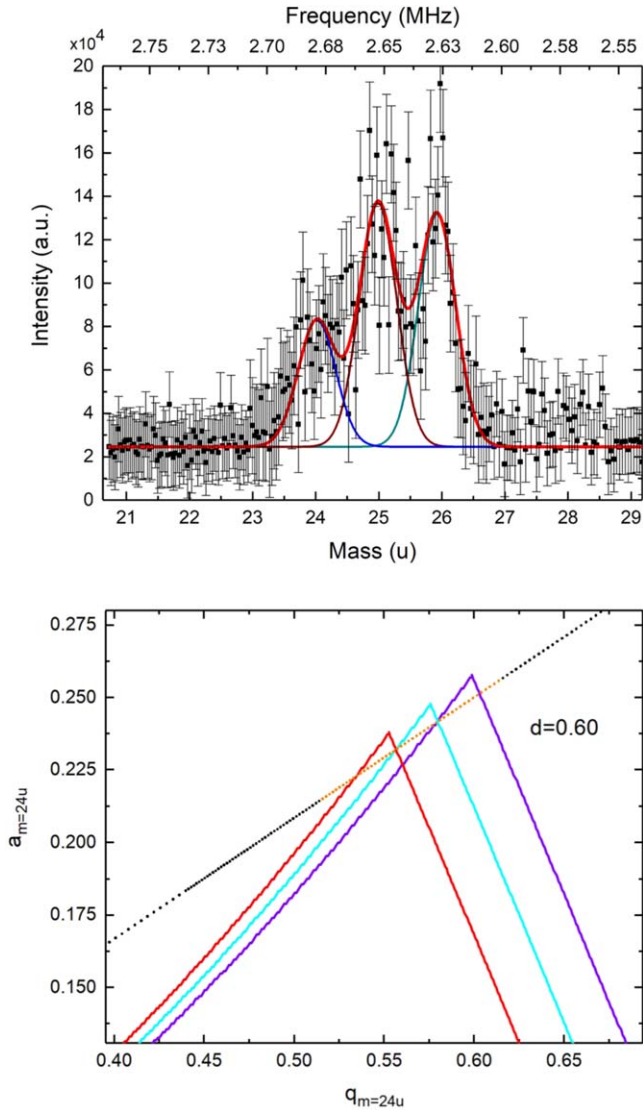


**Figure 5.** (Upper plot) Mass to charge anion spectrum intensity in the DIT for  $d = 0.6$ ,  $V_{rf} = 248$  V,  $V_{ax} = -100$  V. The working slope is scanned from  $\Omega/2\pi = 2.54$ – $2.77$  MHz in steps of 1 kHz (upper  $x$ -axis) corresponding to 23–27 u (lower  $x$ -axis). The spectrum is fitted with three Gaussians of FWHM 1 u with the red line showing their sum. The error bars are given for Poissonian shot noise of the integrated MCP intensity after background subtraction. (Lower plot) Stability diagrams for  $m = 24, 25, 26$  u in red, cyan, purple plotted in Mathieu parameter space of  $m = 24$  u using equation (4). The line indicates the working slope for  $d = 0.6$ , where the orange part shows the same parameter scan range to obtain the spectrum in the upper plot.

subtraction with its shot noise for an average of 60 trapping cycles for masses between  $m = 23$  u and  $m = 27$  u and of 20 trapping cycles for masses outside this range. For each trapping cycle particles are stored for 0.2 ms before being extracted and detected on the MCP. The spectrum shows clear peaks at the masses 24 u ( $C_2^-$ ), 25 u ( $C_2H^-$ ) and 26 u ( $H_2CC^-$ ). The peaks at 25 and 26 u have approximately the same size, while the 24 u peak is found to be about 50% smaller so that it contains around 16% of the trapped particles. In figure 5, the Gaussian fits show that the peaks exhibit an estimated FWHM (resolution) of  $\sim 1$  u. Above the shot

noise, there is also a small contribution visible around mass 27 u, probably corresponding to the stable molecule  $C_2H_3^-$  [46]. Considering the detected signal of produced anions from figure 3, the  $C_2^-$  production yield is on the order of  $\sim 3\%$ . For the same trap operation condition of  $d = 0.6$ , the lower plot of figure 5 shows the theoretical working slope in the stability diagram, defined by equation (6). The orange part of the working slope indicates the experimentally scanned  $\Omega$  range. This plot further shows the edges of the stability diagrams for the masses 24, 25 and 26 u, which are drawn in the  $a - q$  parameter space of the mass 24 u. It can be seen that the spectrum scans through the different masses, where certain  $\Omega$  values can select a single trapped mass. We also expect for certain settings to measure an overlap between the mass contributions, which gives rise to the finite width of the measured mass peaks.

As the gain of the MCP varies depending on the impact velocity and on the molecular chemical reaction at the MCP's surface, only rough absolute particle numbers can be given in our case. The counted number of distinguishable dots from the MCP images corresponds to approximately 100 trapped anions. In [9, 25] about  $10^7$  anionic molecules were produced per valve shot by using the same valve in a similar experiment with 5% ammonia gas in He. Assuming similar discharge conditions in our valve setup, we estimate that  $\sim 10^5$   $C_2^-$  are accelerated per valve shot where the most losses occur during the deceleration of the anion beam. This effect could be reproduced from COMSOL simulations (see figure 2). Furthermore, in [9] the created anions exhibited low internal energies of about 10 meV, which would correspond to a vibrational ground state occupation of the X state of  $C_2^-$  and would be essential for future laser cooling attempts on  $C_2^-$  [21–23].

#### 4. Conclusion

In this article we presented the pulsed production of anionic molecules from a  $C_2H_2$  and  $CO_2$  gas mixture in He via a pulsed discharge valve and subsequent trapping of  $C_2^-$  in a DIT. The mass spectrum up to 70 u of the anions produced by the valve was recorded using a Wien filter. The stability conditions for the DIT were theoretically described and the  $a - q$  stability diagram was measured for values up to  $q < 0.72$  and  $a = \pm 0.3$ . Operating the trap at the edge of the stability diagram, we recorded a mass spectrum of the trapped  $C_2H_x^-$  particles. Here  $C_2^-$  was found to contribute  $\sim 16\%$ , which corresponds to an overall produced yield of  $\sim 3\%$ , and an extrapolated number of  $\sim 10^5$   $C_2^-$  per valve shot from [9]. As the valve can be operated at  $\sim 10$  Hz and the anion pulse length is  $\sim 30$   $\mu$ s, a Penning trap would allow trapping of  $\sim 10^7$   $C_2^-$  within seconds and permits subsequent electron cooling to environmental temperatures. Because  $C_2^-$  was produced from supersonic beam expansion with a discharge inside the nozzle, the gas cools rapidly during the expansion and the collisions of the produced anions with the neutral carrier leave them internally cold [9, 25]. On this basis  $C_2^-$  has been produced with internal energies residing in the vicinity of 10 meV [47, 48]. This indicates that this  $C_2^-$  source is

amply sufficient for laser spectroscopy and laser cooling in rf and Penning traps [22, 23].

## Acknowledgments

We would like to thank Daniel Comparat for valuable discussions.

## ORCID iDs

Sebastian Gerber  <https://orcid.org/0000-0001-5101-1250>

## References

- [1] McCarthy M C, Gottlieb C A, Gupta H and Thaddeus P 2006 *Astrophys. J.* **652** L141–4
- [2] Simons J 2011 *Annu. Rev. Phys. Chem.* **62** 107–28
- [3] Li X and Paldus J 2006 *Chem. Phys. Lett.* **431** 179–84
- [4] Jin D S and Ye J 2012 *Chem. Rev.* **112** 4801–2
- [5] Carr L D, DeMille D, Krens R V and Ye J 2009 *New J. Phys.* **11** 055049
- [6] Smuczyńska S and Skurski P 2008 *Chem. Phys. Lett.* **452** 44–8
- [7] Gabrielse G, Fei X, Orozco L A, Tjoelker R L, Haas J, Kalinowsky H, Trainor T A and Kells W 1989 *Phys. Rev. Lett.* **63** 1360–3
- [8] Deiglmayr J, Goritz A, Best T, Weidemüller M and Wester R 2012 *Phys. Rev. A* **86** 043438
- [9] Luria K, Christen W and Even U 2011 *J. Phys. Chem. A* **115** 7362–7
- [10] Shuman E S, Barry J F and Demille D 2010 *Nature* **467** 820–3
- [11] Hummon M T, Yeo M, Stuhl B K, Collopy A L, Xia Y and Ye J 2013 *Phys. Rev. Lett.* **110** 1–5
- [12] Zhelyazkova V, Cournol A, Wall T E, Matsushima A, Hudson J J, Hinds E A, Tarbutt M R and Sauer B E 2014 *Phys. Rev. A* **89** 2–6
- [13] Kellerbauer A and Walz J 2006 *New J. Phys.* **8** 45
- [14] Ahmadi M *et al* 2017 *Nature* **548** 66–9
- [15] Ahmadi M *et al* 2018 *Nature* **561** 211–5
- [16] Doser M *et al* 2012 *Class. Quantum Grav.* **29** 184009
- [17] Müller H, Peters A and Chu S 2010 *Nature* **463** 926–9
- [18] Pan L and Beck D R 2010 *Phys. Rev. A* **82** 014501
- [19] Walter C W, Gibson N D, Matyas D J, Crocker C, Dungan K A, Matola B R and Rohlén J 2014 *Phys. Rev. Lett.* **113** 1–5
- [20] Cerchiari G, Erlewein S, Yzombard P, Zimmermann M and Kellerbauer A 2019 *J. Phys. B: At. Mol. Opt. Phys.* **52** 155003
- [21] Yzombard P, Hamamda M, Gerber S, Doser M and Comparat D 2015 *Phys. Rev. Lett.* **114** 213001
- [22] Gerber S, Fesel J, Doser M and Comparat D 2018 *New J. Phys.* **20** 23024
- [23] Fesel J, Gerber S, Doser M and Comparat D 2017 *Phys. Rev. A* **96** 031401
- [24] Hillenkamp M, Keinan S and Even U 2003 *J. Chem. Phys.* **118** 8699–705
- [25] Luria K, Lavie N and Even U 2009 *Rev. Sci. Instrum.* **80** 104102
- [26] Fesel J V 2019 Molecular anions as a coolant for antimatter experiments *PhD Thesis* University of Vienna
- [27] Douglas D 2009 *Mass Spectrosc. Rev.* **28** 937–60
- [28] Berton A, Traldi P, Ding L and Brancia F L 2008 *J. Am. Soc. Mass. Spectrom.* **19** 620–5
- [29] Deb N, Pollum L L, Smith A D, Keller M, Rennick C J, Heazlewood B R and Softley T P 2015 *Phys. Rev. A* **91** 1–6
- [30] Konenkov N V, Sudakov M and Douglas D J 2002 *Am. Soc. Mass Spectrom.* **13** 597–613
- [31] Pipes L A 1953 *J. Appl. Phys.* **24** 902–10
- [32] Brabeck G F and Reilly P T A 2014 *Int. J. Mass Spectrom.* **364** 1–8
- [33] Ding L, Sudakov M, Brancia F L, Giles R and Kumashiro S 2004 *J. Mass Spectrom.* **39** 471–84
- [34] Kjærgaard N and Drewsen M 2001 *Phys. Plasmas* **8** 1371–5
- [35] Lykke K R, Murray K K and Lineberger W C 1991 *Phys. Rev. A* **43** 6104–7
- [36] Blondel C, Chaibi W, Delsart C, Drag C, Goldfarb F and Kröger S 2005 *Eur. Phys. J. D* **33** 335–42
- [37] Smith J, Kim J and Lineberger W C 1997 *Phys. Rev. A* **55** 2036–43
- [38] Chipman D M 1978 *J. Phys. Chem.* **82** 1080–3
- [39] Fujii A, Morita S I, Miyazaki M, Ebata T and Mikami N 2004 *J. Phys. Chem. A* **108** 2652–8
- [40] Refaey K M A and Franklin J L 1976 *Int. J. Mass Spectrom.* **20** 4810
- [41] Ervin K M, Anusiewicz I, Skurski P, Simons J and Lineberger W C 2003 *J. Phys. Chem. A* **107** 8521–9
- [42] Knapp M, Echt O, Kreisle D, Mark T D and Recknagel E 1986 *Chem. Phys. Lett.* **126** 225–31
- [43] Zhou J, Garand E and Neumark D M 2007 *J. Chem. Phys.* **127** 154320
- [44] DeVine J A, Weichman M L, Xie C, Babin M C, Johnson M A, Ma J, Guo H and Neumark D M 2018 *J. Phys. Chem. Lett.* **9** 1058–63
- [45] Dressler R and Allan M 1987 *J. Chem. Phys.* **87** 4510–8
- [46] Ellison G B, Engelking P C and Lineberger W C 1978 *J. Am. Chem. Phys.* **100** 2556–8
- [47] de Beer E, Zhao Y, Yourshaw I and Neumark D M 1995 *Chem. Phys. Lett.* **244** 400–6
- [48] Bragg A E, Wester R, Davis A V, Kammrath A and Neumark D M 2003 *Chem. Phys. Lett.* **376** 767–75